J. Phys. B: At. Mol. Opt. Phys. **42** (2009) 035001 (8pp) doi:10.1088/0953-4075/42/3/035001

Landé factors for even-parity 5p*n*p and 5p*n*f J = 1, 2 levels along the Rydberg series of Sn I

Jiaxin Xu[1], Shuai You[1], Ying Zhang[1], Wei Zhang[1], Zhiguo Ma[1], Yanyan Feng[1], Yan Xing[1], Xiangbin Deng[1], P Quinet[2,3], É Biémont[2,3] and Zhenwen Dai[1,3]

[1] Department of Physics, Jilin University, and Key Lab of Coherent Light, Atomic and Molecular Spectroscopy, Ministry of Education, Changchun 130021, People's Republic of China
[2] IPNAS (Bât. B15), Université de Liège, Sart Tilman, B-4000 Liège, Belgium
[3] Astrophysique et Spectroscopie, Université de Mons-Hainaut, B-7000 Mons, Belgium

E-mail: dai@jlu.edu.cn

Received 7 November 2008, in final form 12 December 2008
Published 21 January 2009
Online at stacks.iop.org/JPhysB/42/035001

Abstract
Landé *g*-factors have been measured by time-resolved laser-induced fluorescence and Zeeman quantum-beat techniques for the even-parity levels of the $J = 1$ 5p*n*p ($n = 11$–13, 15–19) and $J = 2$ 5p*n*p ($n = 11$–13, 15–19, 31, 32), 5p*n*f ($n = 4$, 5, 9–19, 22, 23) Rydberg series and for all the 5p7p and 5p8p perturbing levels of neutral tin. A two-colour two-step excitation scheme was used in the experiment. The experimental results have been compared with theoretical *g*-values obtained by the multichannel quantum defect theory and the relativistic Hartree–Fock theory, respectively. In most cases, the theoretical values agree well with the experimental data.

1. Introduction

Investigating the magnetic properties of the atoms is fundamental in many fields of physics, including astrophysics. In particular, a detailed knowledge of the Landé *g*-factors is important to analyse the atomic spectra when an external magnetic field is applied. It can also provide us with useful information regarding the spin–orbit interaction and, consequently, the coupling schemes encountered in atoms. Moreover, the *g*-factor is helpful for the assignment of the energy levels in term analysis and allows us to get a deeper insight into the properties of Rydberg states of atoms.

The ground configuration of neutral tin is $5s^25p^2$ and its Rydberg states consist of a highly excited electron outside of a 5p-electron ionic core. The atom has two ionization limits: $^2P^o_{1/2}$ (59232.69 cm^{-1}) and $^2P^o_{3/2}$ (63484.18 cm^{-1}) [1]. The energy levels of Sn I have been investigated thoroughly in view of the rather simple structure involved in this atom. The early data were summarized by Moore [2], and, later on, the atomic structure of Sn I was studied by Brill [3] and Wilson [4] using an arc discharge and an absorption technique, respectively, but their results were not published. Brown *et al* [1] reported on the high-resolution absorption spectrum of Sn I in the region between 158 and 204 nm and determined many odd-parity levels. Recently, using a two-step excitation technique, numerous $J = 1, 2$ even-parity levels from 5p*n*p and 5p*n*f configurations, as well as many autoionizing levels, were investigated by Nadeem *et al* [5–7]. It should be mentioned that Jin *et al* [8] measured some 5p*n*p and 5p*n*f even-parity Rydberg levels with $J = 0$–3 utilizing the resonant multi-photon ionization and the time-of-flight mass spectroscopy methods, but their detailed results were not published. The $5s5p^3$ configuration of Sn I, which strongly interacts with the $5s^25pns$ and $5s^25pnd$ configurations, has been discussed in detail by Dembczynski *et al* [9, 10].

In comparison to the energy levels, the Landé *g*-factors derived experimentally are still very fragmentary. This results from the difficulties in investigating neutral tin in the laboratory and, more specifically, from the fact that: (1) a high-temperature source is needed to get an atomic beam with sufficient vapour density; (2) for even-parity levels, the intermediate resonance levels used for a two-step excitation can only be excited by UV laser light and have lifetimes of only a few nanoseconds while, for odd-parity states, almost all

[4] Author to whom any correspondence should be addressed.

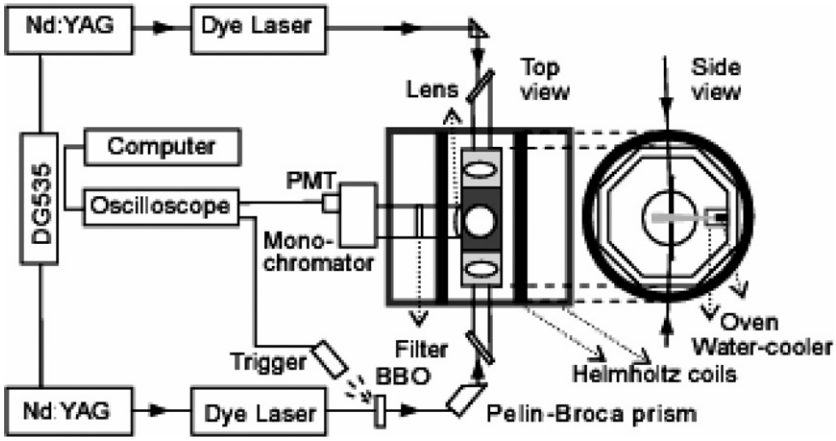

Figure 1. Experimental setup for Landé factor measurements.

the excitations from the ground level need vacuum ultraviolet (VUV) laser light which is somewhat difficult to produce.

Moore [2] summarized all the Landé factors of Sn I that can be found in the literature. These results, deduced from observations of the Zeeman effect by Back [11], Meggers [12], Green and Loring [13], concern only very few odd-parity levels belonging to the 5p6s, 5p5d, 5p7s and 5p6d configurations together with the $5p^2$ levels. To our knowledge, no g-factors for even-parity levels of Sn I except for the $5p^2$ levels have been reported up to now.

As a consequence of this lack of information in Sn I, we report, in the present paper, on the measurements of g-factors for even-parity levels in the 5pnp and 5pnf $J = 1$ and 2 Rydberg series of Sn I using a time-resolved laser-induced fluorescence (TR-LIF) technique and the Zeeman quantum-beat spectroscopy. The g-factors of 37 levels have been obtained. The experimental data were analysed by the multichannel quantum defect theory (MQDT) and by the relativistic Hartree–Fock (HFR) approach so as to get a deeper understanding of the characteristics of the Rydberg series. From the comparison between the experimental and the theoretical results, it has been possible to test the reliability of the theoretical models and their ability to predict new data for high-excitation levels not considered in the present paper or in previous investigations.

2. Experimental setup

The experimental setup used for Landé-factor measurements is shown in figure 1 and the detailed excitation schemes relevant to the present experiment are illustrated in figure 2. A high-temperature oven was mounted at the bottom of a vacuum chamber for providing an atomic beam of sufficient vapour density. It can be operated up to 1700 K. To eliminate the effect of the magnetic field induced by the heating current, the oven was surrounded by two heating molybdenum wires. The oven system was made of corundum. There was a hole of 1.5 mm diameter on the cover of the crucible for generating an atomic beam of low collimation ratio.

A two-step excitation was used in the experiment. Two linearly polarized dye lasers (Sirah Cobra-Stretch) pumped

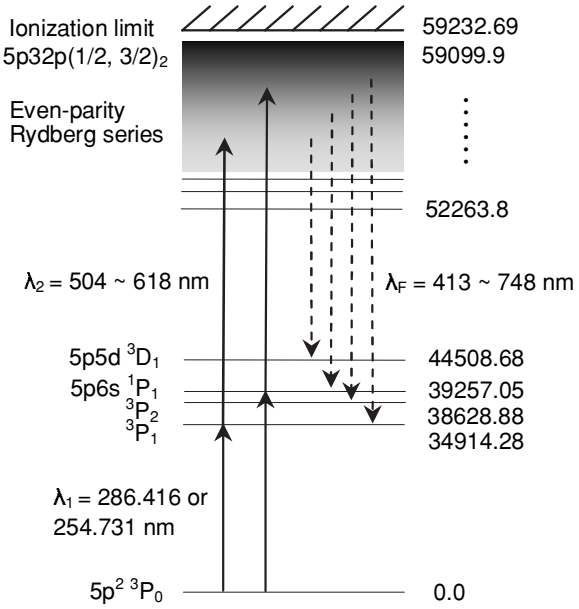

Figure 2. Partial energy-level diagram of the Sn atom and the excitation schemes used in the present work. The solid lines indicate the excitation pathways, and the dashed lines show the fluorescence channels. All the energy levels are expressed in cm^{-1}.

respectively by two Q-switched Nd:YAG lasers (Spectra-Physics Quanta-Ray Pro-Series and Continuum Precision II) working at a 10 Hz repetition rate and with about 8 ns pulse duration were used for excitation. The dye lasers had a linewidth of about 0.08 cm^{-1}. For the first excitation step, a dye laser was focused on a BBO type-I crystal to generate a frequency-doubled light which induced the transitions from the $5p^2\,{}^3P_0$ ground level to the intermediate states. For the second excitation step, the atoms populated on the intermediate level were further excited to the selected even-parity levels by another dye laser. The two laser beams, propagating from opposite directions, crossed at a very small angle at the centre of the vacuum chamber where they interacted with the vertical atomic beam. Since the intermediate resonant level has a lifetime of only several nanoseconds [14], by applying a digital delay generator (Stanford Research System 535), the delay

between the first and the second lasers was adjusted to 3–5 ns in order to produce a sufficiently intense fluorescence. Following the stepwise excitation, the fluorescence signal was focused onto a grating monochromator by a fused silica lens, and then was detected by a photomultiplier tube (PMT) (Hamamatsu R3896) in a direction perpendicular to the laser and to the atomic beams. A 500 MHz digital oscilloscope (Tektronix TDS 620B) was used to register the time-resolved photocurrent signal from the PMT. The oscilloscope was connected through a GPIB cable to a computer in which the signal could be analysed.

A pair of Helmholtz coils was used to generate a homogenous magnetic field which made the investigated levels split into several sublevels, and the direction of the magnetic field was aligned with both the horizontal component of the earth's magnetic field and the direction of the fluorescence detection. The vertical component of the earth's field was counteracted by the other pairs of coils at the top and bottom of the vacuum chamber. The two sets of coils were operated with high-stability constant-current power supplies. The current of the coils was monitored by a digital amperemeter, and the current fluctuation was not beyond 0.1%. The calibration of the horizontal magnetic field was performed by measuring the g-factor of the 6s6p $^3P_1^o$ level of Yb I, the value of which was determined to be 1.4928, with a high precision, by Budick *et al* [15] and Baumann *et al* [16]. The uncertainty of the horizontal magnetic-field calibration was less than 0.1%. The vertical magnetic field was calibrated by a sensitive Gauss meter.

3. Measurement and results

It is well known that a degenerate atomic level will split into several Zeeman sublevels in a magnetic field B. When the intervals between the sublevels are not large, the sublevels can be coherently excited by a pulsed laser, and then they will emit fluorescence modulated in intensity and produce Zeeman quantum beats in a time-resolved signal. In the present experiment, the planes of polarization of the two lasers were chosen perpendicular to each other, so that only sublevels with magnetic quantum numbers ± 1 could be excited since the ground state of Sn I was a $J = 0$ level. The beat frequency ν in the fluorescence signal is related to the field B by $h\nu = 2g\mu_B B$, where h is the Planck constant and μ_B is the Bohr magneton. ν can be determined by a Fourier transform analysis of the fluorescence curve. In order to eliminate the effect of the horizontal component of the earth's magnetic field, the fluorescence quantum-beat curves were recorded in pairs with magnetic fields in opposite directions by changing the current direction in the coils. In front of the monochromator, a polarizer plate was placed for obtaining more prominent quantum beats.

For each level, more than six pairs of curves were registered under different field strengths extending from 4 to 25 gauss and the mean values of the g-factors were adopted as the final results in table 1. The statistical scattering of different measurements and a conservative estimate of the possible systematic errors resulting from the magnetic-field calibration were included in the quoted error bars. As an example, the signal obtained for 13f $(1/2, 5/2)_2$ is shown in figure 3 together with a curve of pure beats obtained by subtracting an exponential decay curve from the signal. In figure 3, the frequency spectrum derived from a Fourier transform of the curve corresponding to pure beats is also presented. The peak frequency in the Fourier spectrum was determined by fitting a Gaussian profile to the peak.

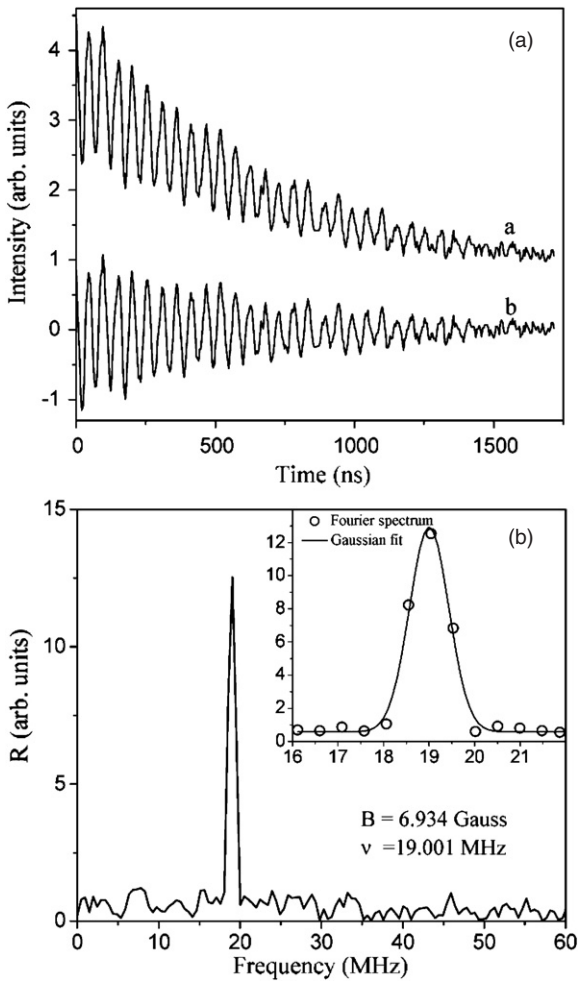

Figure 3. Zeeman quantum-beat recording (a) and the calculated Fourier-transform spectrum (b) for 5p13f $(1/2, 5/2)_2$. In (a), the curve a is a fluorescence decay curve with quantum beats, the curve b is the quantum beats by subtracting the fitted decay curve from the curve a. In (b), the inset shows a Gaussian fit to the principal peak in the Fourier-transform spectrum.

4. HFR calculations

Landé g-factors of energy levels are frequently very sensitive to the coupling conditions and, consequently, their usefulness is enhanced by their relation to g-values in intermediate coupling which is given by

$$g_{\gamma J} = \sum_{\alpha LS} g_{LSJ} |\langle \alpha LSJ | \gamma J \rangle|^2, \qquad (1)$$

where the summation is over the same set of quantum numbers as for the wavefunction $|\gamma JM\rangle$ of the M sublevel of a level

Table 1. Measured Landé g-factors of even parity $J = 1$ and 2 Rydberg levels in Sn I together with comparison with the HFR and MQDT theoretical results.

				g_J factors		
Term[a]	E_{Expt} (cm^{-1})	E_{HFR} (cm^{-1})	E_{MQDT} (cm^{-1})	Experiment	HFR	MQDT
$5p_{1/2}6p\ ^3P_1$	42342.3[b]	42331	42330.3	–	0.694	0.8865
$5p_{1/2}6p\ ^3D_2$	43238.7[b]	43414	43077.4	–	1.184	1.1534
$5p_{1/2}6p\ ^3D_1$	43368.5[b]	43389	43366.5	–	1.344	1.2065
$5p_{3/2}6p\ ^1P_1$	46603.4[b]	46631	46581.2	–	1.113	1.4499
$5p_{3/2}6p\ ^3P_2$	47235.2[b]	47223	47058.9	–	1.327	1.1420
$5p_{3/2}6p\ ^3S_1$	47805.7[b]	47811	47809.6	–	1.852	1.3581
$5p_{3/2}6p\ ^1D_2$	48189.7[b]	48177	48017.2	–	1.159	1.1546
$5p_{1/2}7p\ ^3P_1$	50755.8[b]	50822	50761.3	0.6652(27)[g]	0.672	0.9585
$5p_{1/2}7p\ ^3D_1$	51113.3[b]	51178	51058.6	1.4631(44)[g]	1.454	1.0947
$5p_{1/2}7p\ ^3D_2$	51170.8[b]	51277	51265.6	1.1807(30)[g]	1.179	1.1403
$5p_{1/2}4f\ J = 2$	52263.8[b]	52264	52365.3	0.8759(29)	0.875	0.8811
$8p(1/2, 3/2)_1$	–	54528	51651.5	–	1.394	1.4286
$8p(1/2, 3/2)_2$	–	54521	54264.6	–	1.164	1.1543
$5p_{1/2}5f\ J = 2$	54767.7[b]	54919	54770.7	0.8844(19)	0.882	0.9085
$5p_{3/2}7p\ ^1P_1$	54990.0[b]	54899	54960.1	1.0723(21)[g]	1.102	1.1901
$5p_{3/2}7p\ ^3P_2$	55186.9[b]	55097	55201.8	1.3073(27)[g]	1.368	1.3000
$5p_{3/2}7p\ ^3S_1$	55373.8[b]	55326	55281.6	1.8121(43)[g]	1.818	1.9137
$5p_{3/2}7p\ ^1D_2$	55500.6[b]	55480	55421.6	1.1944(19)[g]	1.136	1.1907
$9p(1/2, 3/2)_1$	–	55946	54139.0	–	1.498	1.5351
$9p(1/2, 3/2)_2$	–	56008	55905.4	–	1.162	1.1457
$6f(1/2, 5/2)_2$	56135.28[d]	56117	56142.8	–	0.882	0.8988
$5p_{3/2}4f\ J = 2$	56396.0[b]	56319	56411.2	–	0.859	0.2826
$5p_{3/2}4f\ J = 1$	56632.9[b]	56459	56636.0	–	0.499	1.3368
$5p_{3/2}4f\ J = 2$	56486.5[b]	56461	56741.4	–	1.099	1.1659
$10p(1/2, 3/2)_1$	–	56741	56794.3	–	1.498	1.3779
$10p(1/2, 3/2)_2$	56828.73[d]	56830	56818.8	–	1.168	1.1656
$7f(1/2, 5/2)_2$	56933.23[d]	56965	56964.1	–	0.886	0.9029
$11p(1/2, 3/2)_1$	57380.0[d]	57380	57386.4	1.4910(26)	1.495	1.3460
$11p(1/2, 3/2)_2$	57399.9[e]	57400	57394.7	1.1713(22)	1.167	1.1555
$8f(1/2, 5/2)_2$	–	57500	57496.2	–	0.887	0.9023
$12p(1/2, 3/2)_1$	57784.3[e]	57784	57785.2	1.4828(34)	1.489	1.3327
$12p(1/2, 3/2)_2$	57792.7[e]	57793	57791.1	1.1708(29)	1.167	1.1563
$9f(1/2, 5/2)_2$	57867.1[c]	57866	57861.3	0.8909(23)	0.888	0.9011
$13p(1/2, 3/2)_1$	58065.7[e]	58066	58066.2	1.4548(45)	1.469	1.3150
$13p(1/2, 3/2)_2$	58071.5[e]	58072	58071.6	1.1708(40)	1.166	1.1579
$10f\ 1/2[5/2]_2$	58123.49[d]	58122	58122.3	0.8852(80)	0.888	0.8999
$14p(1/2, 3/2)_1$	58272.1[e]	58267	58270.0	–	1.047	1.2421
$14p(1/2, 3/2)_2$	58277.7[e]	58281	58276.6	–	1.168	1.1621
$11f\ 1/2[5/2]_2$	58309.04[d]	58308	58314.4	0.8967(34)	0.893	0.9011
$8p(3/2, 1/2)_1$	58327.8[e]	58328	58331.8	1.1397(50)	1.181	1.5344
$8p(3/2, 1/2)_2$	58400.6[f]	58388	58403.9	1.2399(59)	1.238	1.2585
$15p(1/2, 3/2)_1$	58432.0[e]	58432	58435.5	1.5178(82)	1.533	1.5439
$15p(1/2, 3/2)_2$	58442.1[e]	58448	58438.7	1.2321(30)	1.250	1.1599
$12f(1/2, 5/2)_2$	58465.1[f]	58465	58465.3	0.9040(30)	0.897	0.9339
$8p(3/2, 3/2)_1$	58497.6[e]	58501	58497.1	1.7730(69)	1.766	1.0881
$16p(1/2, 3/2)_2$	58542.6[f]	58538	58545.7	1.1869(106)	1.199	1.1938
$16p(1/2, 3/2)_1$	58550.4[e]	58551	58548.1	1.5594(36)	1.499	1.1335
$8p(3/2, 3/2)_2$	58574.0[f]	58596	58568.9	1.0522(56)	1.167	1.0670
$13f(1/2, 5/2)_2$	58583.1[c]	58585	58584.5	1.008(48)	0.965	0.9882
$17p(1/2, 3/2)_1$	58644.2[e]	58644	58643.1	1.5327(112)	1.507	1.5281
$17p(1/2, 3/2)_2$	58653.0[f]	58649	58652.5	1.1586(128)	1.155	1.1444
$14f(1/2, 5/2)_2$	58669.1[f]	58669	58669.0	0.8921(39)	0.889	0.9133
$18p(1/2, 3/2)_1$	58716.1[e]	58716	58716.3	1.5307(139)	1.508	1.4725
$18p(1/2, 3/2)_2$	58727.6[f]	58728	58727.9	1.1699(75)	1.164	1.1490
$15f(1/2, 5/2)_2$	58741.9[f]	58742	58741.5	0.8892(41)	0.889	0.9081
$19p(1/2, 3/2)_1$	58787.30[d]	58787	58776.7	1.5131(115)	1.507	1.5205
$19p(1/2, 3/2)_2$	58789.3[f]	58790	58789.8	1.1628(84)	1.165	1.1507
$16f(1/2, 5/2)_2$	58801.4[f]	58801	58801.1	0.8908(48)	0.888	0.9062
$20p(1/2, 3/2)_1$	58838.78[d]		58828.3	–		1.5103
$20p(1/2, 3/2)_2$	58840.8[f]		58841.0	–		1.1516
$17f(1/2, 5/2)_2$	58850.6[f]	58851	58850.4	0.8919(62)	0.888	0.9051
$21p(1/2, 3/2)_1$	58881.90[d]		58872.3	–		1.4859
$21p(1/2, 3/2)_2$	58883.5[f]		58883.9	–		1.1521

Table 1. (Continued.)

Term[a]	E_{Expt} (cm^{-1})	E_{HFR} (cm^{-1})	E_{MQDT} (cm^{-1})	g_J factors		
				Experiment	HFR	MQDT
$18f(1/2, 5/2)_2$	58891.8[f]	58892	58891.8	0.8884(63)	0.888	0.9044
$22p(1/2, 3/2)_1$	58918.24[d]		58909.8	–		1.4682
$22p(1/2, 3/2)_2$	58920.0[f]		58920.1	–		1.1525
$19f(1/2, 5/2)_2$	58926.8[f]	58927	58926.8	0.8904(29)	0.888	0.9038
$23p(1/2, 3/2)_1$	58949.70[d]		58941.8	–		1.4561
$23p(1/2, 3/2)_2$	58950.7[f]		58950.9	–		1.1528
$20f(1/2, 5/2)_2$	58956.6[f]		58956.6	–		0.9030
$24p(1/2, 3/2)_1$	58976.00[d]		58969.4	–		1.4476
$24p(1/2, 3/2)_2$	58977.3[f]		58977.4	–		1.1530
$21f(1/2, 5/2)_2$	58982.3[f]		58982.3	–		0.9017
$25p(1/2, 3/2)_1$	58999.40[d]		58993.3	–		1.4413
$25p(1/2, 3/2)_2$	59000.3[f]		59000.3	–		1.1533
$22f(1/2, 5/2)_2$	59004.1[f]		59004.5	0.8833(47)		0.8987
$5f(3/2, 5/2)_1$	59014.1[f]		59014.0	–		1.4366
$26p(1/2, 3/2)_1$	59018.82[d]		59032.3	–		1.4329
$26p(1/2, 3/2)_2$	59020.2[f]		59020.3	–		1.1534
$23f(1/2, 5/2)_2$	59026.8[f]		59023.7	0.8728(48)		0.8849
$27p(1/2, 3/2)_2$	59037.6[f]		59037.6	–		1.0624
$27p(1/2, 3/2)_1$	–		59048.3	–		1.4299
$24f(1/2, 5/2)_2$	59042.5[f]		59038.7	–		0.7255
$5f(3/2, 7/2)_2$	59042.5[f]		59044.1	–		0.6408
$28p(1/2, 3/2)_2$	59052.9[f]		59053.3	–		1.1466
$28p(1/2, 3/2)_1$	–		59062.5	–		1.4275
$25f(1/2, 5/2)_2$	59057.1[f]		59056.8	–		0.8884
$29p(1/2, 3/2)_2$	59066.7[f]		59066.8	–		1.1493
$29p(1/2, 3/2)_1$	–		59075.1	–		1.4255
$26f(1/2, 5/2)_2$	59070.1[f]		59069.9	–		0.9016
$30p(1/2, 3/2)_2$	59078.9[f]		59078.9	–		1.1486
$30p(1/2, 3/2)_1$	–		59086.4	–		1.4238
$27f(1/2, 5/2)_2$	59081.9[f]		59081.7	–		0.9056
$5f3/2[3/2]_2$	59084.6[d]		59096.1	–		1.1197
$31p(1/2, 3/2)_2$	59089.5[f]		59089.4	1.1301(104)		1.1432
$31p(1/2, 3/2)_1$	–		59096.5	–		1.4224
$28f(1/2, 5/2)_2$	59092.3[f]		59092.2	–		0.9147
$32p(1/2, 3/2)_2$	59099.9[f]		59100.7	1.1249(122)		1.1555
$32p(1/2, 3/2)_1$	–		59105.6	–		1.4212

[a] Unless otherwise indicated, the designations are from [2, 5, 6, 21] where the corresponding energy levels were reported, the others base on analyses by the multichannel quantum defect theory.
[b] From [2].
[c] Determined in this work.
[d] From [21].
[e] From [5].
[f] From [6].
[g] From [20].

labelled γJ and expressed in terms of LS basis states $|\alpha LSJM\rangle$ by the following formula:

$$|\gamma JM\rangle = \sum_{\alpha LS} |\alpha LSJM\rangle\langle\alpha LSJ|\gamma J\rangle. \quad (2)$$

The $g_{\gamma J}$ value is thus a weighted average of the Landé g_{LSJ} factors, the weighting coefficients being just the corresponding component percentages from the eigenvector of the γJ level in the LS-coupling representation.

In the present work, the Landé g-factors were calculated using the wavefunctions in intermediate coupling generated by the pseudo-relativistic Hartree–Fock method (HFR) developed by Cowan [17] in which we have included core-polarization effects by means of a pseudo-potential depending on two parameters, i.e. the electric dipole polarizability of the ionic core, α_d, and the cut-off radius, r_c [18, 19]. More precisely, our previous calculations, named HFR(B) in [20], were extended to higher values of the principal quantum number up to $n = 19$ for the 5pns, 5pnp, 5pnd, 5pnf and 5png Rydberg series. We were not able to achieve convergence of the self-consistent-field (SCF) process in both HFR and HXR [17] approaches of the Cowan code in the cases of configurations with $n > 19$. The core-polarization parameters were the same as those used in [20], i.e. $\alpha_d = 18.22a_0{}^3$ and $r_c = 2.40a_0$. A semi-empirical adjustment of the computed energy levels to the experimental values taken from [2, 5, 6, 21] was then performed along the different series of interest, i.e. 5pnp $(1/2, 3/2)_1$, 5pnp $(1/2, 3/2)_2$ and 5pnf $(1/2, 5/2)_2$.

5. MQDT analyses

The MQDT approach, first proposed by Seaton [22] and reformulated by Fano [23], has been shown to be a powerful tool for analysing interchannel interactions of perturbed Rydberg series in atoms [24–27]. By fitting the theoretical level energies to the experimental data, MQDT wavefunctions revealing the interchannel interactions can be obtained, which are useful for predicting other spectroscopic properties such as natural radiative lifetimes, Landé factors and hyperfine structures. The details of the theoretical method and the relevant formulation for Landé factor calculation of perturbed Rydberg states with MQDT wavefunctions can be found in [27–30].

The 5pnp and 5pnf $J = 1$ Rydberg series of Sn I consist of five collision channels: 5pnp $(1/2,\ 1/2)_1$, $(1/2,\ 3/2)_1$, $(3/2,\ 1/2)_1$, $(3/2,\ 3/2)_1$ and 5pnf $(3/2,\ 5/2)_1$, while the $J = 2$ series include six channels: 5pnp $(1/2,\ 3/2)_2$, $(3/2,\ 3/2)_2$, $(3/2,\ 1/2)_2$ and 5pnf $(1/2, 5/2)_2$, $(3/2, 5/2)_2$ and $(3/2, 7/2)_2$. Experimental $J = 1$ levels with energies ranging from 42342.3 cm^{-1} to 59090.7 cm^{-1} and $J = 2$ levels from 43238.7 cm^{-1} to 59193.2 cm^{-1} [2, 5, 6] were used in the MQDT analyses for the two series. There are eight and ten perturbers interfering with the $J = 1$ and 2 Rydberg series, respectively. Using a nonlinear minimization method [31], the optimal MQDT parameters and wavefunctions (i.e., the admixture coefficients of the channels) were determined for each series. Also the MQDT theoretical energy levels of the 5pnp (n = 6–32) and 5pnf (n = 4–28) $J = 1$ and 2 series, as deduced for the investigated states, are shown in table 1 (column 3). The root mean squares (rms) deviation between the MQDT and the experimental levels is 28.6 cm^{-1} for the $J = 1$ and 48.4 cm^{-1} for the $J = 2$ levels. If the lowest levels with larger deviations are excluded, the rms deviation is 2.53 cm^{-1} ($J = 1$, eight lowest levels excluded) and 1.86 cm^{-1} ($J = 2$, ten lowest levels excluded), respectively. It should be pointed out that, based on the g_J data as well as on the MQDT wavefunctions, the assignments of the 5p16p $(1/2,\ 3/2)_{1,2}$ levels should be interchanged as shown in table 1.

Using MQDT wavefunctions, the Landé factor g_J^i of the level i can be calculated by

$$g_J^i = \sum_a \left(Z_a^i\right)^2 g_J(a) + \sum_b \left(Z_b^i\right)^2 g_J(b), \tag{3}$$

where a and b denote the perturbed and perturbing channels having the same J and parity, respectively. Z_a^i and Z_b^i are the admixture coefficients of a and b channels, $g_J(a)$ and $g_J(b)$ are the Landé factors relevant to the corresponding channels which are not dependent upon the level i and can be calculated analytically in the pure-coupling representations. When there are two channels converging to the same ionization limit, the angle θ, describing the orthogonal transformation of the two degenerate channels, has no effect on MQDT theoretical energies because the energy values do not contain enough information to depict the properties of the Rydberg levels and to get all the MQDT parameters [28–30]. This will lead to a larger uncertainty in the wavefunctions obtained by the energy fitting procedure. The lifetimes of the Rydberg levels however are generally not dependent upon this uncertainty, while the opposite is true for the g-factors. Therefore, the g-factors can be used to optimize this angle θ in order to improve the MQDT wavefunctions through the obtainment of a new set of Z_a^i. The expression for calculating the g-factor becomes

$$g_J^i = \left(Z_1^i\cos\theta - Z_2^i\sin\theta\right)^2 g_J(1) + \left(Z_1^i\sin\theta + Z_2^i\cos\theta\right)^2 g_J(2) + \sum_b \left(Z_b^i\right)^2 g_J(b). \tag{4}$$

The perturbing channels are usually described in intermediate coupling and hence the g-factors of these channels are difficult to obtain. So it is convenient to consider the g_J factors ($g_J(b)$ in equation (4)) of the perturbing channels as fitting parameters. The intermediate coupling information as well as the modification of the MQDT wavefunctions are contained in the θ angle. g_J optimal parameters can be determined by fitting the theoretical g-factors to the experimental values. $g_J(1)$ and $g_J(2)$ in equation (4) are the analytical Landé factor values of the perturbed channels in pure-coupling schemes.

In pure coupling, the g-factors of the $J = 1$ 5pnp $(1/2,\ 1/2)_1$ and $(1/2,\ 3/2)_1$ series are 0.6667 and 1.5, and those of $J = 2$ 5pnp $(1/2,\ 3/2)_2$ and 5pnf $(1/2,\ 5/2)_2$ series are 1.1667 and 0.8889, respectively. Using equation (4) and the MQDT wavefunctions, theoretical g-factors were fitted to the experimental data of the $J = 1$ and 2 Rydberg series measured in the present work and the following optimal parameters were obtained. For $J = 1$, $\theta = 0.3673$ rad, $g_{Jn\mathrm{p}(3/2,\ 3/2)} = 1.4058$, $g_{Jn\mathrm{f}(3/2,\ 5/2)} = 0.2177$ and $g_{Jn\mathrm{p}(3/2,\ 1/2)} = 2.2060$, while for $J = 2$, $\theta = 3.1472$ rad, $g_{Jn\mathrm{f}(3/2,\ 5/2)} = 1.4951$, $g_{Jn\mathrm{f}(3/2,\ 7/2)} = 0.0307$, $g_{Jn\mathrm{p}(3/2,\ 3/2)} = 1.0972$ and $g_{Jn\mathrm{p}(3/2,\ 1/2)} = 1.3420$. The calculated and measured g_J for the levels up to 5p32p are listed in table 1 and comparisons with the predicted g_J values up to 5p97p are shown in figure 4.

6. Discussion

Landé g-factors of even-parity $J = 1$ 5pnp (n = 7, 11–13, 15–19), $J = 2$ 5pnp (n = 7, 11–13, 15–19, 31, 32) and 5pnf (n = 4, 5, 9–19, 22, 23) Rydberg series as well as of all the 5p7p and 5p8p perturbing levels have been measured. We were not able to perform the measurements for the 5pnp $(1/2,\ 3/2)_{1,2}$ (n = 8–10) and 5pnf (n = 6–8) levels in view of the lack of spectroscopic information for those levels. Also, the g_J value of 5p14p could not be measured because its fluorescence signal was very weak. From the ionization spectra analysed in [5], it was seen indeed that the ionization signal for 5p14p was much weaker than for the neighbouring levels. It is well known that the radiative lifetime of a level increases with the principal quantum number n (scaling according to n^3) and hence the fluorescence intensities become weaker when the energy increases. Therefore, for higher levels only those having short lifetimes can be detected. They are generally located close to the perturbing levels.

A clear fluorescence signal was emitted from a level situated close to 57860 cm^{-1}, but no known level was compatible with this energy. The g-factor of this level was determined to be 0.8909 which is compatible with a level of the 5pnf Rydberg series. But considering that, according to the

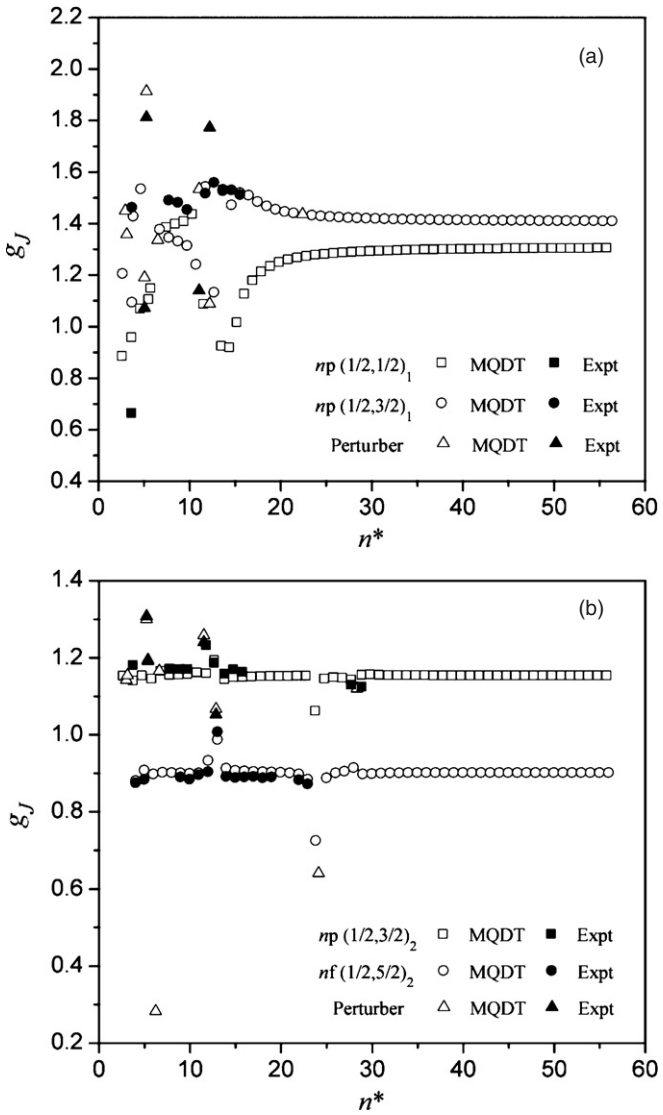

Figure 4. Measured and MQDT Landé factor values versus effective quantum numbers for the $J = 1$ (a) and $J = 2$ (b) Rydberg series of Sn I.

selection rules, the $J = 3$ levels cannot be excited, this level was identified as 5p9f $(1/2,\ 5/2)_2$. The MQDT theoretical analysis also strongly supports this assignment. Similarly, a new level at 58583.1 cm^{-1} has been assigned to $13f$ $(1/2,\ 5/2)_2$.

As seen from figure 4(b), most of the Landé factors along the $J = 2$ series are quite close to the corresponding g_J values obtained in pure coupling schemes, which indicates that the coupling schemes assigned to the $J = 2$ Rydberg series are justified. It is also seen that some g-factors close to the perturbing levels are strongly influenced by the perturbations. Unlike the $J = 2$ series, there exist stronger channel interactions affecting the whole $J = 1$ series, as can be clearly seen in figure 4(a). On the basis of the MQDT analysis, it appears in fact that the two $J = 1$ Rydberg series intensively interact in the energy range considered in the present work, which explains that the g_J values are rather different from those one would expect in pure coupling schemes. These interactions are also observed when considering the behaviour of the line intensities along the $np\ (1/2,\ 1/2)_1$ series as illustrated in figures 3 and 4 of [6].

The HFR Landé factors agree quite well with the experimental data when they are available. They agree also well with the MQDT results if we except the $np\,(1/2,1/2)_1$ $(8 \leqslant n \leqslant 19)$ series for which more discrepancies are observed, the HFR values being closer than the MQDT data to the results that one would obtain in pure coupling. The origin of the discrepancies is not clear and experimental results would be most welcome to decide which theoretical model is the best one. Consequently these two sets of results are not reproduced in table 1 for this series.

7. Conclusion

Landé g-factors of 37 highly lying even-parity $J = 1$ and 2 5pnp and 5pnf Rydberg levels of Sn I have been measured using the time-resolved laser-induced fluorescence technique and the Zeeman quantum-beat spectroscopy. The experimental results have been compared with theoretical data obtained by two independent methods, i.e. the MQDT and HFR approaches. A generally good overall theory-experiment agreement has been achieved except for a few levels. This agreement allows us to assess the predictive power of these approaches for highly excited levels along the Rydberg series in a heavy element like Sn I.

Acknowledgments

We would like to thank Dr Anders Persson (LTH, Lund University, Sweden) for his helpful technical support. This work was supported by the National Natural Science Foundation of China (grant no 10574056) and by the Program for New Century Excellent Talents in University (China). The authors (YX and XD) were supported by the National Fund for Fostering Talents of Basic Science (grant no J0730311). Financial support from the Belgian National Fund for Scientific Research (FR-FNRS) is acknowledged by two of us (EB and PQ) who are Research Director and Senior Research Associate, respectively, of the FRS-FNRS.

References

[1] Brown C M, Tilford S G and Ginter M L 1977 *J. Opt. Soc. Am.* **67** 607
[2] Moore C E 1958 *Atomic Energy Levels* vol III (Washington DC: National Bureau of Standards) NBS Circular No. 467
[3] Brill W G 1964 *PhD Thesis* Purdue University (unpublished)
[4] Wilson J W 1964 *PhD Thesis* Imperial Coll. of Sci. and Tech. of London (unpublished)
[5] Nadeem A, Ahad A, Bhatti S A, Ahmad N, Ali R and Baig M A 1999 *J. Phys. B: At. Mol. Opt. Phys.* **32** 5669
[6] Nadeem A, Bhatti S A, Ahmad N and Baig M A 2001 *J. Phys. B: At. Mol. Opt. Phys.* **34** 2407
[7] Nadeem A, Bhatti S A, Ahmad N and Baig M A 2000 *J. Phys. B: At. Mol. Opt. Phys.* **33** 3729
[8] Jin M, Ding D, Liu H and Pan S 1990 *Inst. Phys. Conf. Ser.* **114** 235
[9] Dembczynski J and Rebel H 1984 *Physica B&C* **125** 341
[10] Dembczynski J and Wilson M 1988 *Z. Phys.* D **8** 329
[11] Back E 1927 *Z. Phys.* **43** 309

[12] Meggers W F 1940 *J. Res. Nat. Bur. Std.* **24** 153
[13] Green J B and Loring R A 1927 *Phys. Rev.* **30** 574
[14] Holmgren L and Svanberg S 1972 *Phys. Scr.* **5** 135
[15] Budick B and Snir J 1967 *Phys. Lett.* A **24** 689
[16] Baumann M and Wandel G 1968 *Phys. Lett.* A **28** 200
[17] Cowan R D 1981 *The Theory of Atomic Structure and Spectra* (Berkeley, CA: University of California Press)
[18] Quinet P, Palmeri P, Biémont É, McCurdy M M, Rieger G, Pinnington E H, Wickliffe M E and Lawler J E 1999 *Mon. Not. R. Astron. Soc.* **307** 934
[19] Biémont É and Quinet P 2003 *Phys. Scr. T* **105** 38
[20] Zhang Y *et al* 2008 *Phys. Rev.* A **78** 022505
[21] Jin M 1991 *PhD Thesis* Jilin University (unpublishd)
[22] Seaton M J 1966 *Proc. Phys. Soc.* **88** 801
[23] Fano U 1975 *J. Opt. Soc. Am.* **65** 979
[24] Armstrong J A, Esherick P and Wynne J J 1977 *Phys. Rev.* A **15** 180
[25] Aymar M, Debarre A and Robaux O 1980 *J. Phys.* B **13** 1089
[26] Hasegawa S and Suzuki A 1996 *Phys. Rev.* A **53** 3014
[27] Dai Z, Li Z S and Zhankui J 2002 *Phys. Rev.* A **65** 022510
[28] Grafström P, Levinson C, Lundberg H, Svanberg S, Grundevik P, Nilsson L and Aymar M 1982 *Z. Phys.* A **308** 95
[29] Aymar M 1984 *J. Opt. Soc. Am.* B **1** 239
Aymar M 1984 *Phys. Rep.* **110** 163
[30] Xingye L, Wanfa L, Zhankui J and Larsson J 1994 *Phys. Rev.* A **49** 4443
[31] Nelder J A and Mead R 1965 *Comput. J.* **7** 308